Journal of Catalysis 276 (2010) 412–422

Contents lists available at ScienceDirect

Journal of Catalysis

journal homepage: www.elsevier.com/locate/jcat

Chitin- and chitosan-anchored methyltrioxorhenium: An innovative approach for selective heterogeneous catalytic epoxidations of olefins

Andrea Di Giuseppe [a], Marcello Crucianelli [a,*], Maurizio Passacantando [b], Stefano Nisi [c], Raffaele Saladino [d,*]

[a] Dipartimento di Chimica, Ingegneria Chimica e Materiali, Università dell'Aquila, via Vetoio, I-67100 Coppito (AQ), Italy
[b] Dipartimento di Fisica and CNR-INFM, Università dell'Aquila, Via Vetoio, I-67100 Coppito (AQ), Italy
[c] Laboratori Nazionali del Gran Sasso, INFN, S.S. 17/bis km 18+910, I-67010 Assergi (AQ), Italy
[d] Dipartimento A.B.A.C., Università della Tuscia, via S.Camillo De Lellis, I-01100 Viterbo, Italy

ARTICLE INFO

Article history:
Received 23 August 2010
Revised 8 October 2010
Accepted 8 October 2010
Available online 10 November 2010

Keywords:
Methyltrioxorhenium
Polysaccharide
Chitosan
Chitin
Heterogeneous catalysis
Olefin oxidation
Hydrogen peroxide

ABSTRACT

Novel complexes between methyltrioxorhenium (MTO) and natural polysaccharides like chitin and chitosan, or modified chitosan-bearing *N*-substituted acyl or alkyl pyridine moieties, were synthesized and used for the oxidation of alkenes, including acid-sensitive styrene derivatives, with urea hydrogen peroxide adduct (UHP) as primary oxidant. High conversions and yields of the corresponding epoxides were obtained. Silica–chitosan hybrid composites with increased surface area and mechanical properties were also prepared and used as MTO supports. A correlation on the role played by the different MTO-coordinating ligand sites of supports, on the experimental outcome of olefin catalytic oxidations, is discussed.

1. Introduction

In the last years, methyltrioxorhenium(VII) ($MeReO_3$, MTO) received a great attention due to the high efficiency in the activation of hydrogen peroxide (H_2O_2) for a large panel of oxidative transformations, including among others, epoxidation of alkenes, oxidation of heteroatoms, Bayer–Villiger rearrangement, or olefin functionalization reactions like olefin metathesis and olefination of aldehydes [1,2]. In addition, MTO showed to be a highly reactive catalyst in nonconventional (*e.g.* ionic liquids or fluorous solvents) or aqueous solvents, providing several advantages from an environmental point of view [1g].

Several attempts have been made to prepare novel heterogeneous catalysts based on the immobilization of MTO on appropriate organic and inorganic supports with the aim to apply this catalyst in industrial processes [1d,1f]. This goal was mainly obtained by the formation of complexes between MTO and ligands containing nucleophilic heteroatoms as anchorage sites. Among them, nitrogen ligands were frequently used to tune the acidity of rhenium during acidic-sensitive synthetic transformations [1b]. Thermodynamic and kinetic studies showed that the stability of MTO complexes strictly depends from the stereoelectronic properties of the ligand, fluxional and dynamical equilibria being effective to decrease the strength of the coordinative bond [2b]. Probably, this is the major reason because of the lack of stereoselective processes based on the use of MTO immobilized on chiral supports [1c]. The properties of complexes between MTO and aromatic amines have been studied in detail, even if the use of non-aromatic ligands, like aliphatic amines or alcohols, is of relevant interest for environmental concerns. This study, to date, represents one of the most stimulating challenges in MTO chemistry [2c,2d]. During our studies devoted on novel rhenium heterogeneous catalysts [3], we described the preparation of nitrogen-based adducts derived from MTO and chiral aliphatic amines and their efficiency in the epoxidation of olefins, with urea hydrogen peroxide complex (UHP) as primary oxidant [4]. With the aim to further evaluate the use of aliphatic amines in the heterogenation process of MTO, we focused our attention on easily available nitrogen-containing polysaccharides like chitin (Ct) (poly-1,4-β-D-*N*-acetyl-glucosamine), an abundant polymer present in crustacean shells, and chitosan (Cs) (poly-1,4-β-D-glucosamine), the deacylated form of chitin. Natural polysaccharides are of industrial interest due to their strong absorption capabilities and affinity for transition metals [5,6], low toxicity, and versatile biotechnological and biocompatible properties [7]. Here, we describe the preparation and structural

* Corresponding authors. Fax: +39 (0)862 433753 (M. Crucianelli), fax: +39 (0)761 357242 (R. Saladino).
E-mail addresses: marcello.crucianelli@univaq.it (M. Crucianelli), saladino@unitus.it (R. Saladino).

0021-9517/$ - see front matter © 2010 Elsevier Inc. All rights reserved.
doi:10.1016/j.jcat.2010.10.003

characterization of novel rhenium catalysts based on the immobilization of MTO on chitosan, chitin and modified chitosan-bearing *N*-substituted acyl and alkyl pyridine moieties [8]. Moreover, to further improve the specific surface area and mechanical properties, chitosan and chitin were also adsorbed on silica gel to generate silica–polysaccharide hybrid composites. Their ability to act as MTO supports was then evaluated. The reactivity of these catalysts was studied in the activation of UHP for the epoxidation of alkenes, including acid-sensitive styrene derivatives. To the best of our knowledge, this is the first report dealing with the use of nitrogen-containing polysaccharides in heterogeneous MTO chemistry.

2. Experimental

2.1. Materials and reagents

Chitin from shrimp shells (product no. C7170) and low molecular weight (M.W.) chitosan (product no. 448869) were supplied by Aldrich. For the chitosan sample, the degree of acetylation (DA = 18%) was determined by pH titration method [9] and by elemental analysis [10]. The calculated value of DA was also confirmed by the ratio between the integrals of, respectively, the acetyl proton signals of *N*-acetyl-D-glucosamine unit (GlcNAc) and the H2 proton signal of glucosamine unit (GlcN), in the corresponding ^{1}H NMR spectrum of chitosan.

All commercial products and solvents were purchased in the highest purity grade available and were used as such. Methyltrioxorhenium(VII), UHP, and olefins 1–5 were purchased from Aldrich. ^{1}H and ^{13}C NMR spectra were recorded on a Bruker (AC-200 MHz) instrument. Gas chromatography–mass spectrometry (GC–MS) analyses of the reaction products were performed using a Varian 2000 GC-MAS instrument, with a 30 m × 0.32 mm × 0.25 μm film thickness (cross-linked 5% phenylmethylsiloxane) column and chromatography-grade helium as the carrier gas. Yields and conversions of the reactions were quantified using *n*-octane as internal standard. In GC calculations, all peaks amounting to at least 0.5% of the total products were taken into account. When necessary, ^{1}H and ^{13}C NMR analyses of products were performed after flash-chromatographic purification on columns packed with silica gel (230–400 mesh) and compared with authenticated samples. Mass spectra were recorded with an electron beam of 70 eV. For the scanning electron microscopy (SEM) photographs, samples were spitter-coated with gold (20 nm).

2.2. Preparation of N-substituted chitosan polymers

2.2.1. Preparation of nicotinoyl chitosan derivatives (NCs)

To a flask containing a solution of 10.0 mL of *N,N*-dimethylacetamide (DMA) and 1.0 g of LiCl, 100 mg of chitosan (0.62 mmol, based on glucosamine unit) was added and mixture heated at 90 °C, until complete solubilization. The solution was then cooled at −18 °C and added, portionwise, with freshly treated sodium hydride (NaH) (60 mg, 2.50 mmol). Once the effervescence ceased (after ca. 1 h), the mixture was warmed at room temperature (r.t.), added with diisopropylethylamine (DIPEA) (2.6 mL, 14.88 mmol), and then treated with nicotinoyl chloride used as hydrochloride salt (1.36 g, 7.44 mmol). The resulting viscous mixture was allowed to stir at 40 °C, overnight. Then, the crude was quenched with a saturated aqueous solution of ammonium chloride, filtered and the solid washed in a Soxhlet apparatus with water, then with acetone, newly filtered and finally dried on P_2O_5, under vacuum, affording a creamy white powder (80% yield).

2.2.2. Preparation of N-alkyl pyridyl chitosan derivatives: N-(3-pyridylmethyl) chitosan (3PCs) and N-(4-pyridylmethyl) chitosan (4PCs). General procedure

A flask containing 500 mg of chitosan (3.10 mmol, based on glucosamine unit) suspended in 50.0 mL of ethanol was refluxed, while stirring, for 20 min. After cooling, the mixture was added with an excess of the corresponding aldehyde (3-pyridinecarboxaldehyde for 3PCs or 4-pyridinecarboxaldehyde for 4PCs, respectively) (1.2 mL, 12.41 mmol) and refluxed for 15 h, under vigorous stirring. After filtration, the crude was washed in a Soxhlet apparatus with methanol and then with acetone, in order to remove excess of aldehyde. Afterwards, the imine function was reduced by the addition of a 2:1 excess of $NaBH_4$ (235 mg, 6.20 mmol) to a water (15.0 mL) suspension of previously obtained imine derivative and allowed, under stirring, for 12 h, at r.t. The same work-up, as above described, followed by a prolonged drying on P_2O_5, under vacuum, afforded the final product (88% yield).

2.3. Preparation of silica–chitosan hybrid composite

One gram of chitosan was suspended in a flask containing an aqueous solution of acetic acid (60 mL, 1.5%) and the mixture heated at 50 °C. After solubilization (*ca.* 1.5 h), 4.50 g of silica (70–230 mesh) was added portionwise, under stirring. After about 30 min, chitosan was precipitated on silica surface by increasing the pH of the mixture (with dropwise addition of NaOH 4.0 M) until pH 13. The hybrid composite was recovered by simple filtration and washed with water to pH 8. Solid was first heated at 373 K for 12 h and then dried on P_2O_5, under high vacuum, affording 4.0 g of powder. The product was finely ground prior to use.

2.4. Preparation of silica–chitin hybrid composite

A solid mixture formed by 2.0 g of chitin and 4.0 g of silica (70–230 mesh) was ground in a ball mill for 12 h at 60 °C affording quantitatively a homogeneous creamy white powder.

2.5. Preparation of heterogeneous catalysts: general procedure

To a flask containing 1.0 mL of selected solvent (I: CH_2Cl_2, II: THF, III: EtOH or IV: H_2O, respectively), 40.0 mg of the appropriate polysaccharide (Ct, Cs, NCs, 3PCs or 4PCs, respectively) was added and the suspension left at r.t., under stirring, for 2 h, in order to allow the swelling of matrix. Then, 25.0 mg of MTO [0.1 mmol, corresponding to a theoretical value of the loading factor (L.F., defined as mmol of MTO supported per gram of polysaccharide) = 2.5, and to a (2:1) *N* matrix/MTO molar ratio, respectively] was added and the mixture allowed to stir, at r.t., for 12 h. After centrifugation, the brown solid was washed and carefully dried under nitrogen flux and then under high vacuum, affording the appropriate heterogeneous catalysts. In the case of hybrid–polysaccharide composites, the procedure used for heterogenization of MTO was as follows: to a flask containing 4.0 mL of selected solvent (I–IV), 200.0 mg of the appropriate hybrid composite (SiO_2Cs or SiO_2Ct, respectively) was added and the suspension left at r.t., under stirring, for 2 h, in order to allow the swelling of matrix. Then, 50.0 mg of MTO (0.2 mmol, theoretical L.F. = 1.0) was added, and the mixture was allowed to stir, at reflux, for 2–4 h. After centrifugation, the same work-up as above described was performed, affording the corresponding catalyst (MTO/SiO_2Cs I–IV or MTO/SiO_2Ct I–IV, respectively). The actual L.F. values of catalysts were measured by ICP-MS analysis (see onward).

2.6. Catalyst characterization

2.6.1. Surface area evaluation

Surface areas of Cs, Ct, and hybrid composites like silica–chitosan SiO_2Cs and silica–chitin SiO_2Ct samples were measured by a BET nitrogen adsorption method, working with an Asap 2000 Micromeritics instrument (Table 1).

2.6.2. Estimation of degree of N-substitution by ^{1}H NMR spectroscopy

The degree of *N*-substitution (DS) was determined using ^{1}H NMR spectroscopy as shown in Eq. (1). The *N*-acetyl peak of GlcNAc unit was used as internal reference, working with D_2O/CF_3COOD (1%) as solvent. The measurements were done at r.t., without water suppression, using 15 mg of sample in 0.5 mL of solvent.

$$\mathrm{DS}\ (\%) = \{(\mathrm{Ar}/n)/[\mathrm{H2} + 1/3\mathrm{NHAc}]\} \times 100 \quad (1)$$

where DS (%) is the degree of *N*-substitution, Ar is the integral area of aromatic protons, *n* is the number of aromatic hydrogen atoms per substituent, H2 is the integral areas of the protons at C-2 carbon of GlcN unit, and NHAc is the integral area of NAc protons (Table 1) [11a].

2.6.3. Fourier-transform infrared spectroscopy (FTIR)

Attenuated total reflection infrared (ATR-IR) spectroscopic analyses were recorded, at room temperature, in the range of 4000–650 cm^{-1}, using a Perkin–Elmer Spectrum One spectrometer equipped with an ATR-IR cell. IR spectra were recorded by averaging 32 scans, with a resolution of 4 cm^{-1}.

2.6.4. Inductively coupled plasma mass spectrometry (ICP-MS)

ICP-MS analyses were performed on a ICP-MS Agilent 7500a spectrometer. Few milligrams of samples were mineralized in closed fluorinated ethylene propylene (FEP) vials using microwave-assisted acid digestion technologies (CEM MDS-2100 model) following the modified method EPA 3052. Samples were digested with 1 ml of 20% HNO_3 aqueous solution, at 150 °C. The solution obtained after mineralization was diluted with deionized water in order to have Re concentration in the ng/g range before ICP-MS measurements. A 10^{-3} g/g certified standard rhenium solution (AccuStandard Lot Number B4065078) was used to calibrate the instrumentation. The relative uncertainties in rhenium concentration given with one standard deviation are in the order of 5%. All recovery test results, considering the uncertainties of the measurements, were compatible with 100%.

2.6.5. X-ray photoelectron spectroscopy (XPS)

The chemical state, of the different elements of Cs and MTO/Cs I samples, was analyzed using a X-ray photoelectron spectroscopy (XPS) system (PHI 1257), equipped with a hemispherical analyzer. The X-ray was generated by a non-monochromatized Mg source ($h\nu$ = 1253.6 eV), and the measurement was taken at an ultrahigh vacuum at about 5×10^{-8} Pa. All the reported binding energy (BE) data have been calibrated using the residual carbon present on the powder samples, positioned at a BE of 285.0 eV. The analysis of XPS data was performed using the XPS Peak Fitting Programme version 4.1 [11b]. The Re 4f, O 1s, N 1s, and C 1s features were detected and analyzed.

Table 1
Characterization data of supports.[a]

Sample	DS (%)[b]	BET (m^2/g)	Elemental analysis		
			C (%)	H (%)	N (%)
Cs	–	1.81 ± 0.06	41.94	6.37	7.68
Ct	–	8.90 ± 0.06	44.79	6.39	6.66
SiO_2Cs	–	358.7 ± 0.5	10.09	2.16	1.75
SiO_2Ct	–	352.5 ± 0.4	n.e.	n.e.	n.e.
3PCs	51	n.e.	49.83	6.46	9.01
4PCs	55	n.e.	50.78	6.32	9.30
NCs	48	n.e.	40.38	6.03	7.07

[a] n.e. = not evaluated.
[b] See Section 2.6.2.

2.6.6. Elemental analysis

The carbon, hydrogen, and nitrogen contents of catalysts were determined by elemental analysis performed with a Fisons Instruments 1108 CHNS-O Elemental Analyzer (Table 1).

2.7. General catalytic oxidative procedure

To a flask containing 0.2 mmol of selected olefin dissolved in 2.0 mL of ethanol, 0.4 mmol of UHP was added, followed by an appropriate amount of catalyst corresponding to 1.0 mol% of MTO with respect to substrate (2.0 mol% in the case of silica-hybrid composites), and the mixture allowed to stir, at r.t., for 36 h. Every 12 h, 0.2 mmol of oxidant was added to the mixture until reaching the total excess of 1.0 mmol (5:1, referred to starting olefin), and the progress of oxidation was monitored by GC–MS analysis, on micro samples (1.0 μL) of reaction mixture withdrawn at periodic time intervals. At the end of the reaction, the catalyst was recovered by filtration and washed with CH_2Cl_2. A small amount of MnO_2 (2.0 mg) was added to eliminate the excess of primary oxidant: the composition of the reaction mixture was found to be unchanged after the addition of MnO_2. Then, the suspension was filtered once again and the filtrate dried over anhydrous Na_2SO_4. After evaporation of the solvent, the crude product was analyzed by GC–MS analysis and, when necessary, purified by flash chromatography. Identity of products was confirmed by ^{1}H and ^{13}C NMR analyses. Spectra were compared with those of authentic compounds.

3. Results and discussion

3.1. Preparation of polysaccharide/MTO heterogeneous catalysts

Initially, the attention was focused on the preparation of heterogeneous MTO catalysts based on the immobilization of MTO on commercially available chitin (Ct) and chitosan (Cs) polysaccharides. As a general procedure, the polysaccharide was suspended in a selected panel of solvents, including organic solvents with a different polarity (I: CH_2Cl_2; II: THF; III: EtOH), and water (IV: H_2O). The appropriate amount of MTO (corresponding to the amount of MTO necessary for a theoretical L.F. = 2.5, with a N_{matrix}/MTO molar ratio value = 2:1) was added and the system carefully stirred for 12 h at r.t. (for details, see Section 2). The catalysts MTO/Cs I–IV and MTO/Ct I–IV were recovered as brownish powder by centrifugation (Scheme 1, route a and b, respectively). In one selected case (with solvent IV: H_2O), the MTO/Cs and MTO/Ct catalysts were also prepared with a higher value of the N_{matrix}/MTO molar ratio = 1:1, to afford compounds MTO/Cs IV* and MTO/Ct IV*.

Chitosan was successively derivatized, at the amino groups, with pyridinyl moieties to further tune the stereolelectronic properties of the support. In particular, *N*-alkyl pyridinyl chitosan derivatives like *N*-(pyridin-3-ylmethyl) chitosan 3PCs and *N*-(pyridin-4-ylmethyl) chitosan 4PCs were prepared through a partial modification of a previously reported procedure [12]. Briefly, a solution of Cs in ethanol was treated with the appropriate aldehyde (3-pyridinecarboxaldehyde for 3PCs or 4-pyridinecarboxaldehyde for 4PCs, respectively) followed by reduction with sodium borohydride ($NaBH_4$) (Scheme 2, route a). MTO/3PCs I–IV and MTO/4PCs

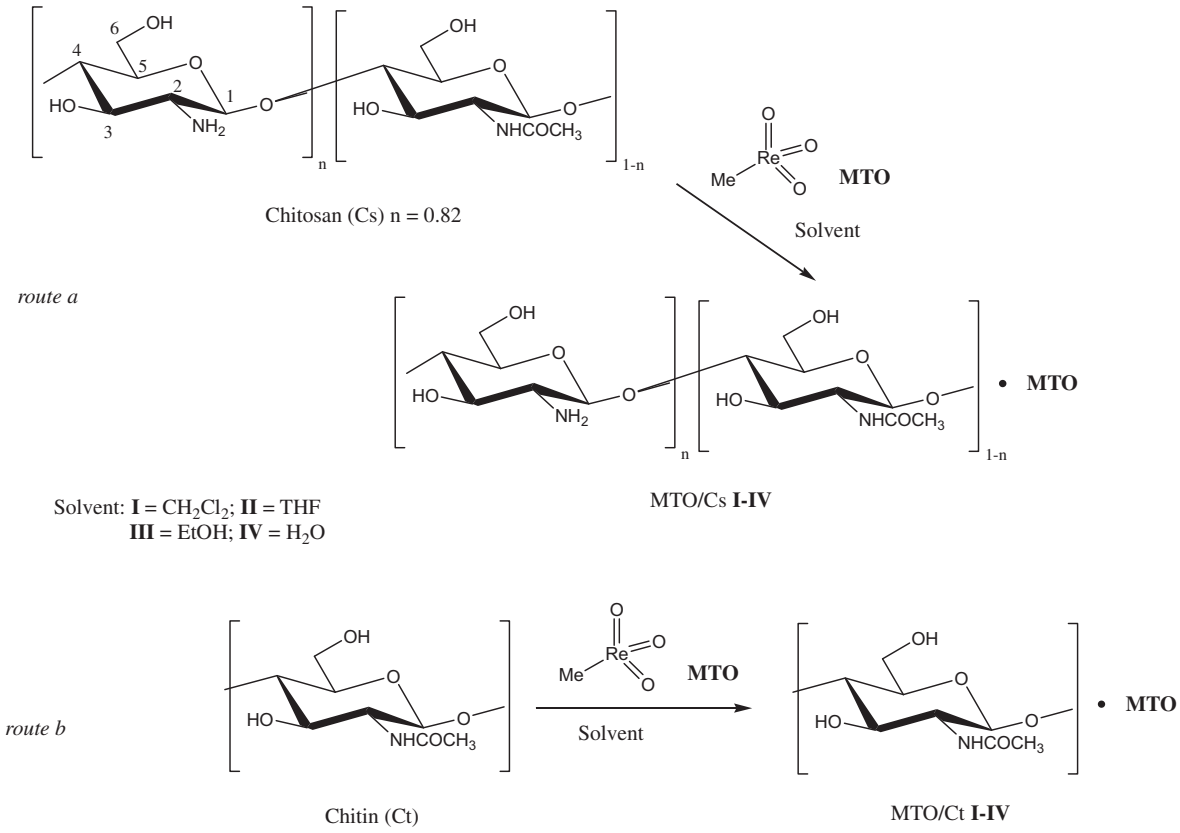

Scheme 1. Schematic drawing for the preparation of MTO/Cs I–IV and MTO/Ct I–IV heterogeneous catalysts.

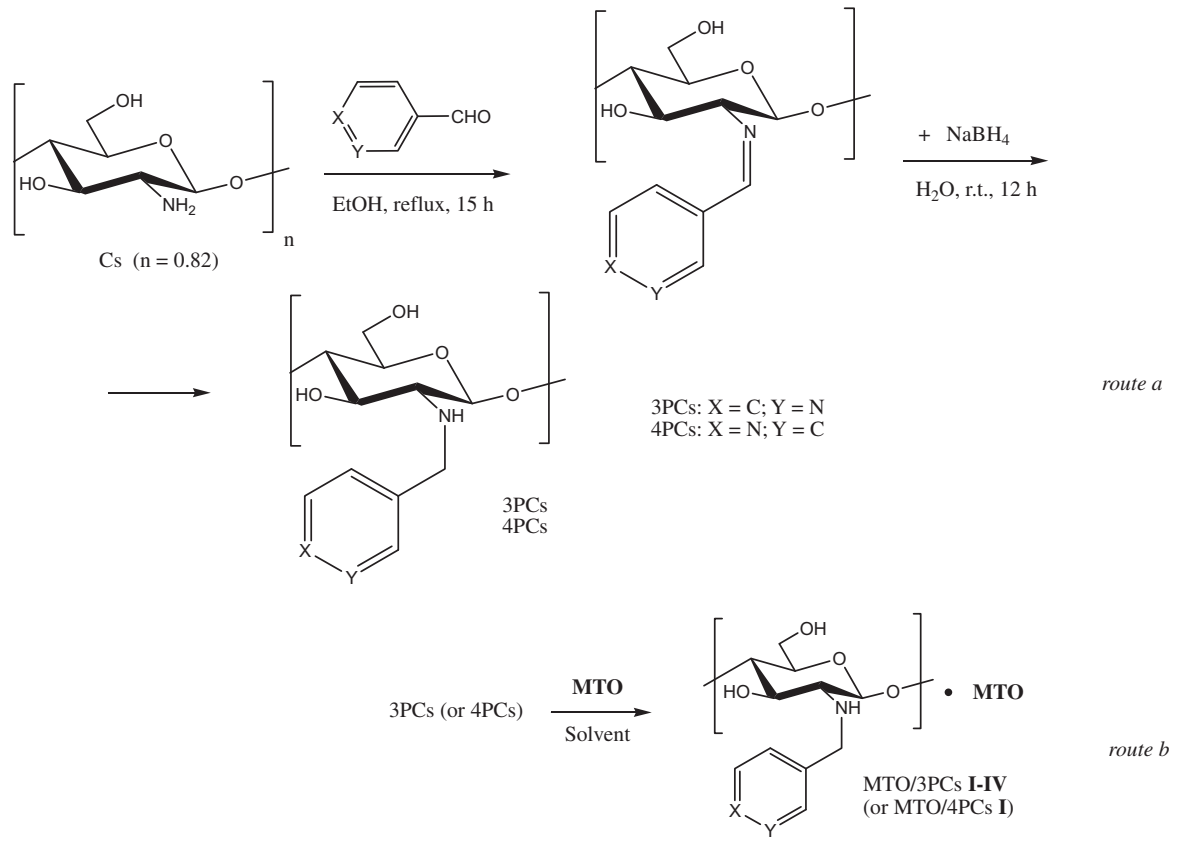

Scheme 2. Schematic drawing for the preparation of derivatized chitosan 3PCs and 4PCs and their use as support for the preparation of heterogeneous catalysts MTO/3PCs I–IV and MTO/4PCs I.

I were then synthesized in accordance with the procedure previously described for catalysts MTO/Cs I–IV (Scheme 2, route b).

In a similar way, nicotinoyl chitosan NCs, in which the pyridin-3-yl functional group is linked to the glucosamine unit by both an amide and/or an ester moieties, was prepared by reacting a DMA/LiCl solution of chitosan with NaH, followed by acylation with nicotinic acid chloride (Scheme 3, route a) [13,14]. MTO/NCs I–IV were then prepared in accordance with the general procedure previously described for catalysts MTO/Cs I–IV (Scheme 3, route b). In this case, the acylation occurred both on alcoholic and amino groups, as evaluated by FT-IR spectra [15].

The L.F. values of novel heterogeneous catalysts were calculated on the basis of their ICP-MS analyses and are reported in Table 2. Generally, values of L.F. in the range of 0.4–5.0 units (Table 2, entries 1–19) were observed depending on the nature of the support and on the polarity of the solvent employed during the preparation of the catalyst, Cs being a support for MTO better than Ct. This was, probably, due to the larger nucleophilic properties of the amino moiety (Cs) than that of the amido moiety (Ct). In both cases, the highest L.F. values were obtained in H_2O and in THF (see for example Table 2, entries 2 and 4–5, and entries 7 and 9–10, respectively). A similar result was observed in the case of *N*-functionalized 3PCs, 4PCs, and NCs supports, so suggesting a better swelling ability of these solvents. Again, the catalyst-loading efficiency in modified Cs was higher than in parent Cs (see for example Table 2, entry 12 versus entry 2) in accordance with the increased ligand capability of the derivatized support. The high efficiency of H_2O in the preparation of catalysts is of relevant interest for what it concerns the environmental impact on the overall process.

Silica–polysaccharide hybrid composites of chitosan and chitin were prepared in accordance with previously reported procedures

Table 2
Loading factors (L.F.s) of novel heterogeneous catalysts.[a]

Entry	Catalyst[b]	Re (ppm)[c]	MTO (% w/w)	L.F.[d]
1	MTO/Cs I	118,000	15.8	0.75
2	MTO/Cs II	157,000	21.0	1.06
3	MTO/Cs III	125,000	16.7	0.80
4	MTO/Cs IV	260,000	34.8	2.14
5	MTO/Cs IV*[e]	417,000	55.8	5.07
6	MTO/Ct I	82,700	11.1	0.50
7	MTO/Ct II	103,000	13.8	0.65
8	MTO/Ct III	71,900	9.6	0.42
9	MTO/Ct IV	112,000	15.0	0.70
10	MTO/Ct IV*[e]	145,000	19.4	0.96
11	MTO/3PCs I	184,000	24.6	1.31
12	MTO/3PCs II	283,000	37.9	2.43
13	MTO/3PCs III	214,000	28.6	1.61
14	MTO/3PCs IV	247,000	33.1	1.71
15	MTO/4PCs I	186,000	25.0	1.34
16	MTO/NCs I	140,000	18.7	0.92
17	MTO/NCs II	285,000	38.1	2.48
18	MTO/NCs III	110,000	14.7	0.70
19	MTO/NCs IV	243,000	32.6	1.95
20	MTO/SiO_2Cs I	55,100	7.4	0.33
21	MTO/SiO_2Cs II	68,000	9.1	0.40
22	MTO/SiO_2Cs III	38,600	5.2	0.22
23	MTO/SiO_2Cs IV	125,000	16.7	0.81
24	MTO/Ct IV*[f]	143,000	–	–

[a] Calculated by ICP-MS analysis on about 5.0 mg of freshly prepared sample.
[b] Prepared from I: CH_2Cl_2; II: THF; III: EtOH and IV: H_2O.
[c] Quantitative profile calculated using a certified standard rhenium solution (see Section 2).
[d] Actual L.F., evaluated after ICP-MS analysis.
[e] Corresponding to a theoretical stoichiometric N_{matrix}/MTO = 1:1 molar ratio.
[f] Catalyst sample recovered after the second recycling step.

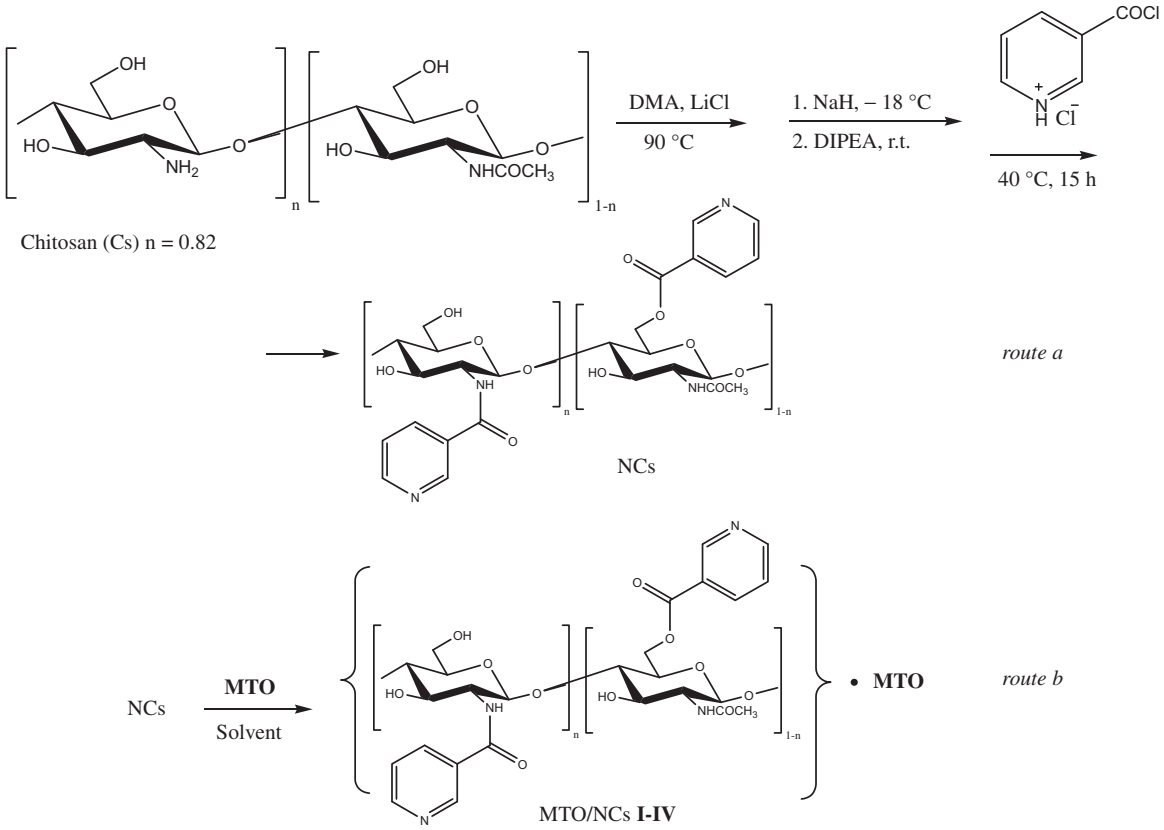

Scheme 3. Schematic drawing for the preparation of derivatized chitosan NCs and its use as support for the preparation of heterogeneous catalysts MTO/NCs I–IV.

[16]. Briefly, Cs solubilized in acetic acid (1.5% aqueous solution) at 50 °C was precipitated on silica surface by increasing the pH of the mixture (with NaOH 4.0 M) to pH 13. In the case of Ct, a different procedure (grinding) was applied due to the low solubility in acidic medium [17]. In particular, the solid mixture of Ct and silica (70–230 mesh) was ground and heated, in a ball mill, for 12 h at 60 °C. The hybrid composite SiO_2Ct was used without further purification. MTO/SiO_2Cs I–IV and MTO/SiO_2Ct I–IV were then prepared using previously described procedures, by stirring the appropriate amount of MTO (corresponding to a theoretical value of the L.F. = 1.0, see Section 2) with hybrid-polysaccharide composites for 5.0 h, at reflux (Scheme 4, route a and b, respectively).

The L.F. values for catalysts MTO/SiO_2Cs I–IV are reported in Table 2 (entries 20–23). Note that the presence of silica significantly inhibits the coordination of MTO on polysaccharides in I–III solvents, with the only exception of SiO_2Cs in H_2O, in which case a value of L.F. comparable to that observed for the other systems was obtained. This result was probably due to the reduced swelling properties of polysaccharide when adsorbed on silica. Unfortunately, values of L.F. for MTO/SiO_2Ct I–IV were found to be too much low for any synthetic interest (values not shown in Table 2).

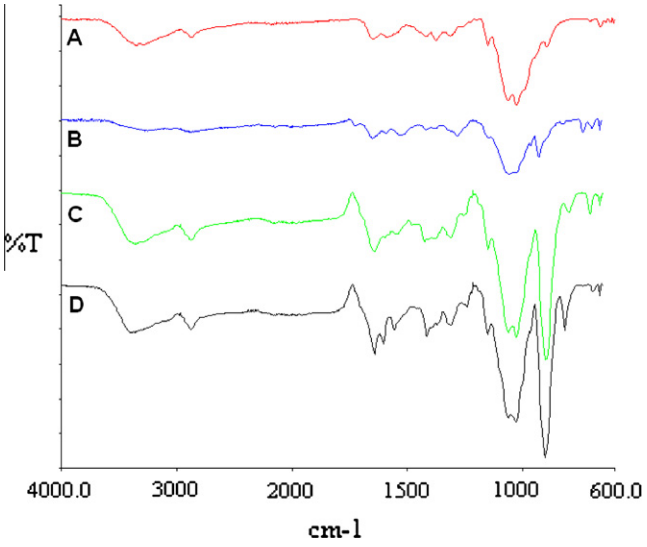

Fig. 1. Infrared spectra of Cs (A) and of heterogeneous catalysts MTO/NCs (B), MTO/3PCs (C), and MTO/4PCs (D).

3.2. Structure characterization of polysaccharide/MTO heterogeneous catalysts

Novel heterogeneous catalysts were characterized by infrared spectroscopy analysis (FT-IR), ^{1}H NMR spectroscopy, and scanning electron microscopy (SEM). The X-ray photoelectron spectroscopy (XPS) analysis was also performed in the selected case of catalyst MTO/Cs I.

The FT-IR spectra of native chitosan (Fig. 1A), with a DA = 18%, showed the typical broad peak centered at around 3330 cm^{-1} corresponding to the stretching of NH_2 and OH groups, the peak at 2873 cm^{-1} attributed to the C—H stretching, that at 1651 cm^{-1} for the stretching of secondary amide (amide I band), along with the N—H bending vibration of amino group at 1599 cm^{-1} [18]. 3PCs and 4PCs showed FT-IR spectra similar to Cs. Anyway, the *N*-derivatization of Cs was confirmed by the appearance of the C=C stretching and C—H bending (out of plane) at 1559, 1578, and 1604 cm^{-1}, and at 797–815 cm^{-1}, respectively, characteristic of the aromatic rings [19]. In the case of NCs, FT-IR spectra showed amide I, amide II, and amide III bands at 1637 cm^{-1}, 1524 cm^{-1}, and 1281 cm^{-1}, respectively, characteristic of secondary amide moiety, besides to C=O stretching at 1723 cm^{-1} for the ester group. In Table 3 are reported the values of the stretching vibrational frequency found for the Re=O double bond [ν(ReO)] for catalysts prepared in CH_2Cl_2. The ν (Re=O) vibration is expected to shift to lower frequencies, in the presence of electron-donating ligands (amine and amide functions of Cs and Ct supports, respectively), on the basis of the theoretical valence-bond resonance structures for the Re—O bond [20].

The assignment of the vibrational frequencies of the R–ReO_3 and R–ReO_3/ligand systems has been described previously [21]. All complexes showed lower ν(ReO) frequencies compared with MTO, equal to 998 cm^{-1} for the symmetric stretching vibration mode and to 959 cm^{-1} for the asymmetric stretching vibration mode [22]. As reported in Table 3, the ν(Re=O) frequencies of 3PCs, 4PCs, and NCs are higher than that of Cs (Fig. 1 and Table 3, entries 3–5 versus entry 1), suggesting a slightly less efficient coordination of MTO. In the case of MTO/NCs I, the ν(Re=O) stretching frequency (Table 3, entry 5) was comparable with that observed for previously synthesized poly-4-vinylpyridine/MTO systems [3a].

Supporting matrices Cs, 3PCs, and 4PCs were characterized also by ^{1}H NMR spectroscopy (Fig. 2). As a general pattern, Cs spectrum

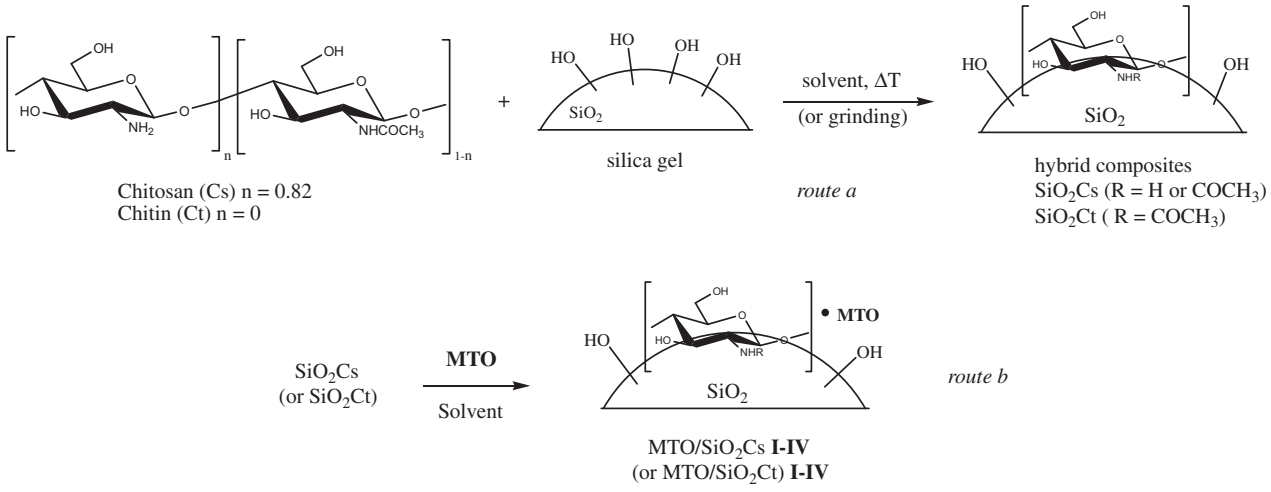

Scheme 4. Preparation of silica–polysaccharide hybrid composites of chitosan and chitin and their use as support for the preparation of heterogeneous catalysts MTO/SiO_2Cs I–IV and MTO/SiO_2Ct I–IV.

Table 3
Selected vibrational frequencies [ν(ReO)] for heterogeneous catalysts prepared in CH_2Cl_2.[a]

Entry	Catalyst	νRe=O (cm^{-1})
1	MTO/Cs I	898
2	MTO/Ct I	899
3	MTO/3PCs I	902
4	MTO/4PCs I	904
5	MTO/NCs I	930
6	MTO/SiO_2Cs I	923

[a] Data recovered at r.t.

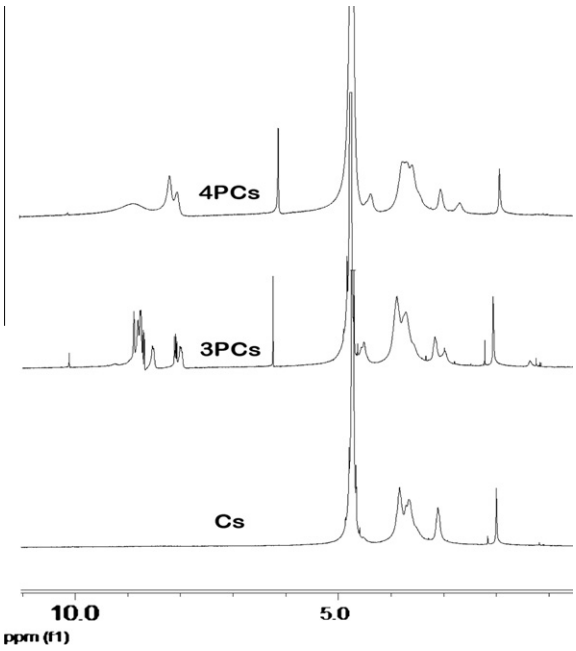

Fig. 2. ^{1}H NMR spectra of Cs and of its derivatives 3PCs and 4PCs.

showed the multiplet at δ 4.0–3.4 ppm due to H3, H4, H5, and H6 protons of glycosidic ring (GlcN), and two singlets at 3.1 and 2.0 ppm (H2 proton of GlcN and the N-acetyl protons of GlcNAc, respectively). The H1 proton signal at δ 4.8 ppm partially falls below the water signal (numbering of atoms is reported in Scheme 1). 3PCs spectrum is characterized by signals of the aromatic protons of a typical *m*-substituted pyridine moiety at δ 9.0–7.9 ppm, besides a broad signal centered at ca. δ 4.5 ppm, attributable to *N*-CH_2 protons of alkylated chitosan, along with a minor singlet at 6.2 ppm, probably due to a low amount of residual imine proton.

A set of scanning electron microscopy (SEM) photographs showing the morphology of the surface of particles of catalysts MTO/Cs IV, MTO/Ct IV, MTO/3PCs I–IV, MTO/NCs IV, and MTO/SiO_2Cs IV are reported in Figs. 3–6. Catalysts MTO/Cs IV and MTO/Ct IV (Fig. 3) are characterized by irregular aggregates with sheets superimposed like structures.

Noteworthy, MTO/3PCs IV shows a different morphology with a complex network of filamentous rubber like fragments (Fig. 4, left side) and a partial helicoidal shape visible at higher magnification (Fig. 4, right side). This latter morphology can be finely tuned by the nature of the solvent used for the preparation of the catalyst, since a well-defined thin flake structure was observed for MTO/3PCs I–III (Fig. 5).

Finally, a typical glass shape morphology was observed in the case of catalyst MTO/SiO_2Cs IV (Fig. 6).

3.3. X-ray photoelectron spectroscopy (XPS)

In Fig. 7, we report the comparison of XPS spectra of Cs (a) and of MTO/Cs I (b) and relative decomposed bands obtained by fitting procedure. The BEs of the decomposed bands shown in Fig. 7 correspond to the BEs listed in Table 4 for O 1s, N 1s, C 1s, and Re 4f bands, for Cs and MTO/Cs I, respectively.

From Table 4, we can verify that BEs of oxygen 1s and carbon 1s peaks were not significantly affected after MTO heterogenation, in accordance with results previously observed for Cu(II), Mo(VI), and Cr(VI) metal ions supported on chitosan [23]. Differently, in the case of nitrogen 1s peak, a new weak band appears at around 402 eV as a result of charge transfer from amine moiety to the metal center, after MTO heterogenation [23]. In the case of MTO/Cs I, for the Re 4*f* region of Fig. 7b, we have fitted the obtained spectrum into two different double peaks due to $4f_{7/2}$ and $4f_{5/2}$ levels, with a spin orbit splitting of 2.4 eV. The BE peak positions at 46.4 and 44.3 eV were assigned to the Re $4f_{7/2}$ levels for Re^{7+} and $Re^{5+/4+}$species, respectively. Therefore, the most intense peak of the Re 4*f* raw data, corresponding to BE of about 46 eV, is considered as the sum of Re $4f_{7/2}$ peak for the Re^{7+} species and of Re $4f_{5/2}$ peak for the Re^{4+} species [24]. Similar results were also observed, by us, in the case of XPS spectra of either catalyst MTO/SiO_2Cs I or authentic MTO samples (not shown), so suggesting that a partial reduction of MTO during XPS experiments was operative (Fig. 7). An analogous behavior was already observed during XPS analyses of polyaniline-supported MTO complexes [25].

3.4. Catalytic activity studies

The catalytic activity of MTO heterogeneous catalysts was evaluated in the epoxidation of olefins, including acid-sensitive styrene derivatives 1–4 and cyclooctene 5 (Scheme 5). The oxidation was optimized in the case of *cis*-β-methyl styrene 3, as a selected substrate, using an amount of catalyst corresponding to 1.0 mol% of MTO with respect to substrate, UHP as primary oxidant in ethanol,

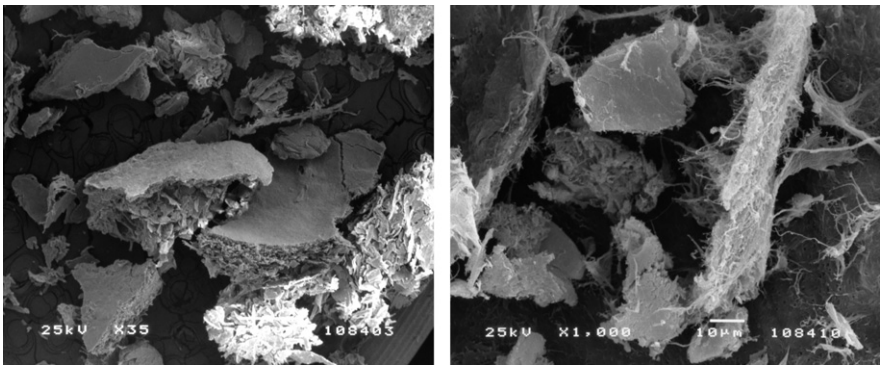

Fig. 3. Scanning electron microscopy (SEM) micrographs of the catalysts MTO/Cs IV (left) and of MTO/Ct IV (right).

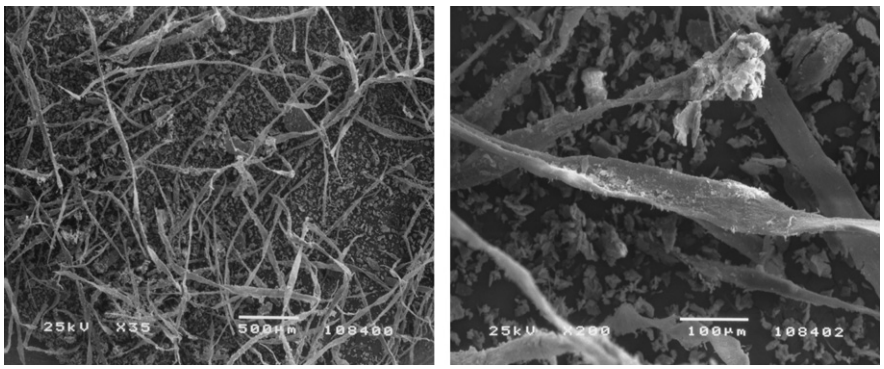

Fig. 4. Scanning electron microscopy (SEM) micrographs of MTO/3PCs IV catalyst at, respectively, lower (left) and larger (right) magnification.

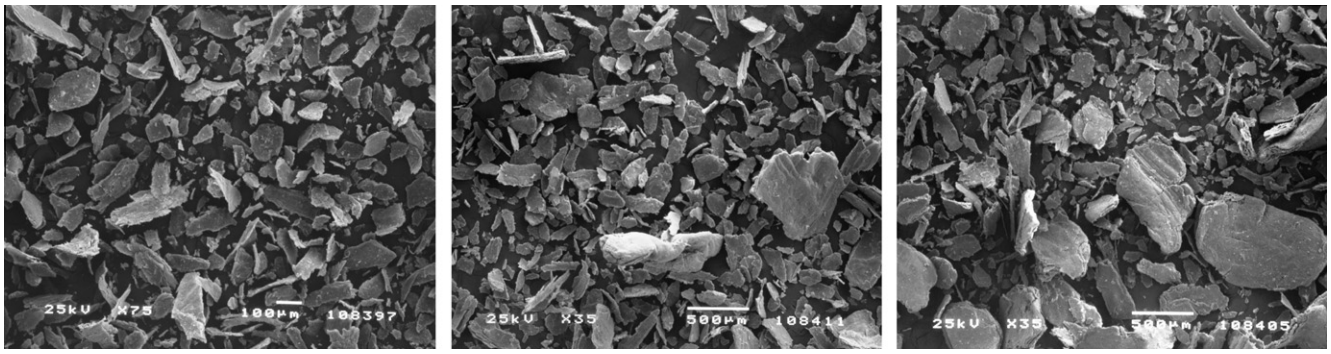

Fig. 5. Scanning electron microscopy (SEM) micrographs of, respectively, MTO/3PCs I (left), MTO/3PCs II (center), and MTO/3PCs III (right) catalysts.

for 36 h at r.t, under moisture (details are furnished in Section 2) [4]. Irrespective of experimental conditions, the β-methyl styrene epoxide 8 was obtained, as the only recovered product, from low to high yield (4–98%). Conversion values and reaction yields are reported in Table 5.

In the absence of the catalyst, less than 5% conversion of substrate took place, under otherwise identical conditions.

As a general reaction pattern, MTO/Ct I–IV were more reactive than parent MTO/Cs I–IV (Table 5, entries 1–5 versus entries 6–10) and, in both cases, catalysts prepared in H_2O were the best catalytic systems. This order of reactivity is in accordance with data previously reported on the effect of nitrogen ligand basicity on the stability and reactivity of supported MTO adducts [4]. In fact, the basicity of amido moiety in Ct is lower than that of the amino moiety in Cs. Moreover, the activity of the catalyst was found to increase by increasing the amount of loaded MTO (see for example Table 5, entry 4 versus entry 5). It is interesting to note that MTO/3PCs I–IV characterized by additional methyl 3-pyridinyl moieties as anchorage sites were more reactive than corresponding MTO/Cs I–IV (Table 5, entries 1–4 versus entries 11–14). In this context, MTO/4PCs I, bearing the methyl 4-pyridinyl moiety, also showed to be an efficient catalyst in the epoxidation of 3 (Table 5, entry 15), suggesting that the position of the nitrogen atom on the pyridine ring was not a crucial factor for the reactivity. Some qualitative structure activity relationships can be outlined by comparison of reactivity data of MTO/NCs I–IV catalysts with those of MTO/3PCs I–IV, which differ only by the oxidation state of the side-chain linker (that is 3Py-CH_2-NH- versus 3Py-CO-NH-) (Table 5, entries 16–19 versus entries 11–14). In particular, MTO/NCs I–IV were more reactive than MTO/3PCs I–IV probably due to the different basicity of the nitrogen atom in the linker and to the presence of the carbonyl moiety as a further coordination site. Finally, the hybrid composite MTO/SiO_2Cs IV was more reactive than parent MTO/Cs IV (Table 5, entry 4 versus entry 20), showing that the activity of the catalyst can be increased by increasing the specific surface area and the mechanical properties of the support. In this latter case, a quantitative conversion of substrate and yield of epoxide was observed with the stoichiometric value of the molar ratio N_{matrix}/MTO (Table 5, entry 21 versus entry 20).

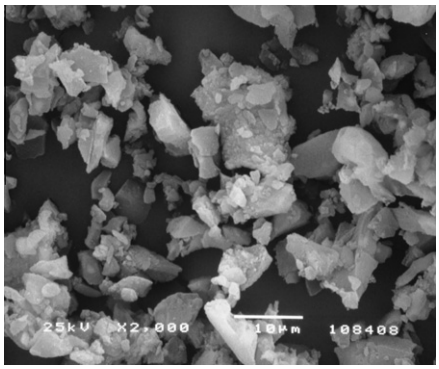

Fig. 6. Scanning electron microscopy (SEM) micrograph of MTO/SiO_2Cs IV catalyst.

In a test for checking the leaching of the catalysts, the oxidation of 3 with MTO/Cs IV* and MTO/Ct IV* was stopped at *ca.* 50% of the final conversion (evaluated by GC–MS analysis of the run). After removal of the catalyst by centrifugation, the colorless solution lost the catalytic activity, indicating that no appreciable amount of MTO had been removed from the polysaccharide matrix; this was also confirmed by the absence of the typical signal of MTO in the ^{1}H NMR spectrum of the corresponding recovered crude solution.

Presumably, the high catalyst activity observed for the heterogeneous MTO systems is to be ascribed to the formation of the known reactive monoperoxo [MeRe(O)$_2$(O$_2$)] and bisperoxo [MeRe(O)(O$_2$)$_2$] η^2-rhenium complexes, even in the presence of the support [2a]. This hypothesis is in part confirmed by the

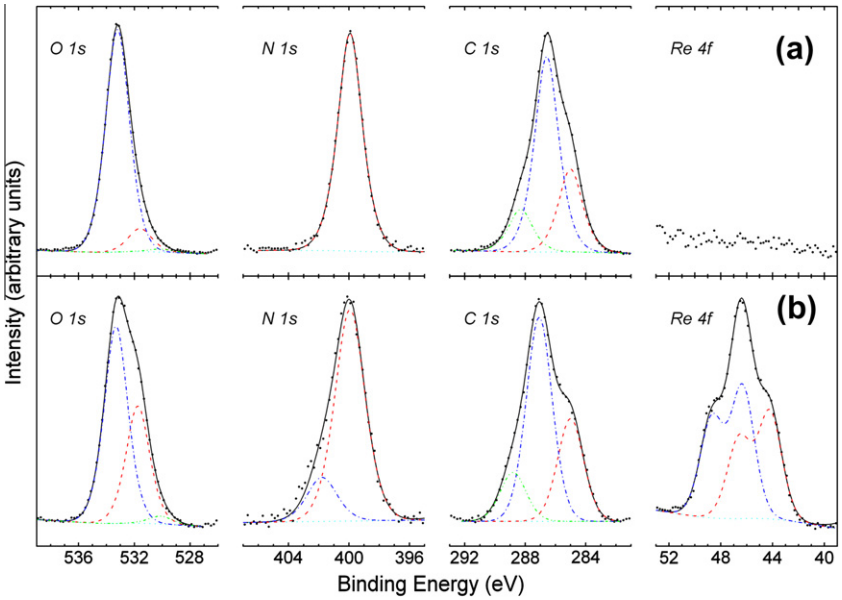

Fig. 7. XPS of O 1s, N 1s, C 1s, and Re 4f core level spectra of Cs (a) and of heterogeneous MTO/Cs I catalyst (b), and decomposed components obtained from fitting procedure.

Table 4
BEs evaluated by XPS analysis on Cs and MTO/Cs I, with relative assignments.[a]

Element	System		Assignments
	Cs	MTO/Cs I	
O 1s	530.2	530.2	O—H
	531.6	531.7	C=O or C—O—C and O—Re
	533.2	533.3	>C—O
N 1s	399.9	400.0	N—H
	–	401.9	Interaction between Cs and MTO
C 1s	285.0	285.0	C—C or contaminated carbon
	286.6	287.1	C—N or C—O or C—O—C
	288.3	288.8	C=O or O—C—O
Re $4f_{7/2}$	–	44.3	$Re^{5+/4+}$
	–	46.4	Re^{7+}

[a] BEs measured in eV units.

appearance of a pale yellow color on the surface of the catalysts after the addition of UHP, which is a very characteristic feature for the formation of active peroxo rhenium species [26].

Among the most reactive catalysts, MTO/Ct IV*, MTO/NCs II and IV, and MTO/SiO_2Cs IV were selected to perform the epoxidation of olefins 1–2 and 4–5 under similar experimental conditions (Scheme 5). Conversion values and reaction yields are reported in Table 6. Again, in the absence of the catalyst, less than 5% conversion of substrate took place under otherwise identical conditions.

Irrespective of experimental conditions, the oxidation of olefins 4–5 afforded the corresponding epoxides 9 and 12 as the only recovered product from acceptable to very good yield (42–97%), MTO/Ct IV* being the best catalytic system (Table 6, entries 3–4). The epoxidation of styrene and α-methyl stryrene 1–2 showed a different selectivity affording products of nucleophilic ring opening, 10–11, besides to epoxides 6–7. These data are in accordance

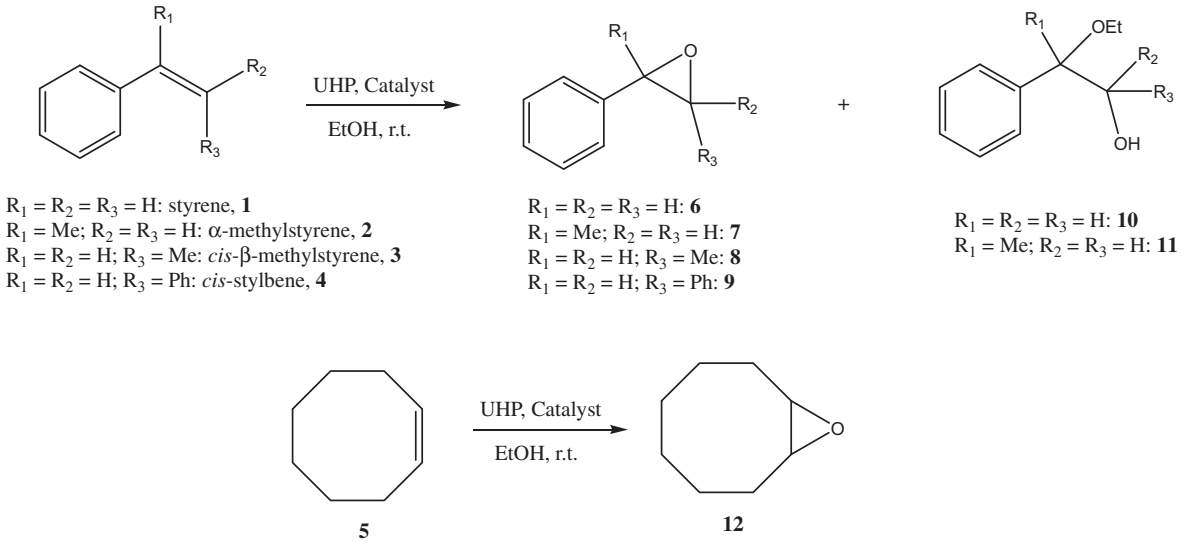

Scheme 5. Heterogeneous catalytic epoxidation of olefins 1–5.

Table 5
Oxidation of *cis*-β-methyl stryrene 3 with heterogeneous MTO-based catalysts and UHP, in EtOH at r.t.

Entry	Catalyst[a]	Conversion (%)	Yield (%)[c]
1	MTO/Cs I	13	11
2	MTO/Cs II	5	4
3	MTO/Cs III	6	5
4	MTO/Cs IV	23	21
5	MTO/Cs IV*,[b]	67	66
6	MTO/Ct I	52	52
7	MTO/Ct II	26	25
8	MTO/Ct III	41	39
9	MTO/Ct IV	70	70
10	MTO/Ct IV*,[b]	98	98
11	MTO/3PCs I	71	70
12	MTO/3PCs II	35	33
13	MTO/3PCs III	54	53
14	MTO/3PCs IV	37	35
15	MTO/4PCs I	63	62
16	MTO/NCs I	74	74
17	MTO/NCs II	92	91
18	MTO/NCs III	58	58
19	MTO/NCs IV	97	96
20	MTO/SiO_2Cs IV	49	48
21	MTO/SiO_2Cs IV*,[b]	98	98

[a] Prepared from I: CH_2Cl_2; II: THF; III: EtOH and IV: H_2O; for actual L.F. values see Table 1.
[b] Corresponding to a theoretical N_{matrix}/MTO = 1:1 stoichiometric molar ratio.
[c] Yields are referred to mmol of product per mmol of starting material.

with the results previously obtained during the oxidation of 1–2 with adduct between MTO and low molecular weight amines and confirm the known high reactivity and low stability of the α-methyl styrene oxide [4]. Analogously with that observed during the oxidation of 3, hybrid composite MTO/SiO_2Cs IV catalyst showed a similar reactivity, in the oxidation of olefins 1–2 and 4, in terms of conversion values (compares Table 6, entries 13–15 versus Table 5, entry 20). Noteworthy, independently of the type of catalyst employed, cyclooctene 5 acted as the most reactive olefin, affording the corresponding epoxide 12 with complete selectivity (Table 6, entries 4, 8, 12 and 16).

Finally, our efforts were aimed at recycling the catalysts. The oxidation of cyclooctene 5 with MTO/Ct IV* was performed as selected example. Catalyst MTO/Ct IV* was used in a successive run, without any further purification, showing the expected reactivity (conversion: 95%; yield of epoxide 12: 93%). However, a decrease in catalyst reactivity (while retaining an high selectivity) was observed during a further successive run (second recycling step; conversion: 79%; yield of epoxide 12: 75%).

Since traces of MTO were not detected by ^{1}H NMR analysis in the crude after work-up of the reaction, it is reasonable to suggest that the decrease in reactivity might be due to a partial degradation of the catalyst to low reactive rhenium species [4,27]. The ICP-MS analysis of catalyst MTO/Ct IV* after the third run confirms this possibility, showing a substantially unmodified total amount of rhenium on the matrix (Table 2, entry 24 versus entry 10).

Table 6
Oxidation of olefins 1–2 and 4–5 with heterogeneous MTO-based catalysts and UHP, in EtOH at r.t.

Entry	Catalyst[a]	Olefin	Product(s)	Conversion%	Yield(s) (%)[b]
1	MTO/Ct IV*[c]	1	6 (10)	83	64 (19)
2	MTO/Ct IV*[c]	2	7 (11)	98	4 (94)
3	MTO/Ct IV*[c]	4	9	95	95
4	MTO/Ct IV*[c]	5	12	97	97
5	MTO/NCs II	1	6 (10)	38	30 (8)
6	MTO/NCs II	2	7 (11)	83	10 (73)
7	MTO/NCs II	4	9	48	48
8	MTO/NCs II	5	12	84	84
9	MTO/NCs IV	1	6 (10)	39	33 (6)
10	MTO/NCs IV	2	7 (11)	67	9 (58)
11	MTO/NCs IV	4	9	62	62
12	MTO/NCs IV	5	12	97	97
13	MTO/SiO_2Cs IV	1	6 (10)	41	38 (3)
14	MTO/SiO_2Cs IV	2	7 (11)	53	7 (46)
15	MTO/SiO_2Cs IV	4	9	42	42
16	MTO/SiO_2Cs IV	5	12	86	86

[a] Prepared from I: CH_2Cl_2; II: THF; III: EtOH and IV: H_2O; for actual L.F. values see Table 1.
[b] Yields are referred to mmol of product per mmol of starting material.
[c] Corresponding to a theoretical N_{matrix}/MTO = 1:1 stoichiometric molar ratio.

4. Conclusions

MTO was efficiently supported on natural nitrogen-containing polysaccharides like chitin and chitosan, as well as, on chitosan derivatives 3PCs, 4PCs, and NCs, where the polysaccharide has been functionalized at the amino moieties. In the case of Cs, the rhenium atom is coordinated at the aliphatic amino group, as shown by the shift of the N 1s band (Δ of 1.9 eV) observed in the XPS spectra. This shift corresponds to the formation of positively charged nitrogen sites during the formation of the complex. As expected on the basis of the theoretical valence-bond resonance structures for the Re—O bond, the stretching vibration frequency values of the Re=O moiety in the FT-IR spectra of all MTO-based heterogeneous catalysts shifted toward lower frequencies in comparison with MTO alone, so confirming an efficient coordination of it with the anchorage sites. The presence of the pyridinyl moiety also affects the morphology of the particles of the catalyst that appears to be characterized by a well-organized filamentous rubber-like structure. The novel MTO heterogeneous compounds were efficient catalysts for the activation of UHP in the epoxidation of olefins, including acid-sensitive styrene derivatives. The order of reactivity was finely tuned by the basicity of the ligand group on the support. In fact, Ct-based catalysts were more reactive than Cs systems, according with the known low basicity of the amido moiety. Finally, *N*-functionalized Cs catalysts were the most active systems, confirming the benign role of aromatic heterocyclic ligands, such as pyridine and pyridine derivatives, in the coordinative chemistry of MTO. Interestingly, in the case of chitosan, the activity of the MTO-based heterogeneous catalyst was found to be increased after the deposition process on silica. The possibility of synthesizing MTO/polysaccharide-anchored heterogeneous catalysts, with the aim to prepare valuable catalysts to be used in the selective epoxidation of olefins, highlights the current interest of natural nitrogen-containing polymers in rhenium synthetic chemistry.

Acknowledgements

University of L'Aquila, University of Viterbo and ASI are acknowledged for the financial support.

References

[1] (a) C.C. Romao, F.E. Kuhn, W.A. Herrmann, Chem. Rev. 97 (1997) 3197;
(b) F.E. Kuhn, A.M. Santos, W.A. Herrmann, Dalton Trans. (2005) 2483;
(c) F.E. Kuhn, J. Zhao, W.A. Herrmann, Tetrahedron: Asymmetry 16 (2005) 3469;
(d) C. Freund, W.A. Herrmann, F.E. Kuhn, in: Organometallic Oxidation Catalysis, Topics in Organometallic Chemistry, vol. 22, Springer, Berlin, 2007, p. 39;
(e) W.A. Herrmann, A.M.J. Rost, J.K.M. Mitterpleininger, N. Szesni, S. Sturm, R.W. Fischer, F.E. Kuhn, Angew. Chem. Int. Ed. 46 (2007) 7301;
(f) K.R. Jain, F.E. Kuhn, J. Organomet. Chem. 692 (2007) 5532;
(g) M. Crucianelli, R. Saladino, F. De Angelis, ChemSusChem 3 (2010) 524.

[2] (a) W.A. Herrmann, R.W. Fischer, W. Scherer, M.U. Rauch, Angew. Chem. Int. Ed. 32 (1993) 1157;
(b) S.M. Nabavizadeh, A. Akbari, M. Rashidi, Eur. J. Inorg. Chem. 12 (2005) 2368;
(c) P. Altmann, F.E. Kuhn, J. Organomet. Chem. 694 (2009) 4032;
(d) S. Yamazaki, Org. Biomol. Chem. 8 (2010) 2377.
[3] (a) R. Saladino, V. Neri, A.R. Pelliccia, R. Caminiti, C. Sadun, J. Org. Chem. 67 (2002) 1323;
(b) G. Bianchini, M. Crucianelli, C. Crestini, R. Saladino, Top. Catal. 40 (2006) 221;
(c) A. Goti, F. Cardona, G. Soldaini, C. Crestini, C. Fiani, R. Saladino, Adv. Synth. Catal. 348 (2006) 476;
(d) R. Saladino, C. Crestini, M. Crucianelli, G. Soldaini, F. Cardona, A. Goti, J. Mol. Catal. A 284 (2008) 108;
(e) A. Di Giuseppe, M. Crucianelli, F. De Angelis, C. Crestini, R. Saladino, Appl. Catal. B 89 (2009) 239.
[4] S. Vezzosi, A. Guimerais, M. Crucianelli, C. Crestini, R. Saladino, J. Catal. 257 (2008) 262.
[5] (a) E. Guibal, Prog. Polym. Sci. 30 (2005) 71;
(b) D.J. Macquarrie, J.J.E. Hardy, Ind. Eng. Chem. Res. 44 (2005) 8499.
[6] (a) M.N.V. Ravi Kumar, R.A.A. Muzzarelli, C. Muzzarelli, H. Sashiwa, A.J. Domb, Chem. Rev. 104 (2004) 6017;
(b) M. Rinaudo, Prog. Polym. Sci. 31 (2006) 603;
(c) K. Kurita, Mar. Biotechnol. 8 (2006) 203.
[7] (a) H. Sashiwa, S.-i. Aiba, Prog. Polym. Sci. 29 (2004) 887;
(b) A. Gandini, Macromolecules 41 (2008) 9491;
(c) T. Kean, M. Thanou, Adv. Drug Deliv. Rev. 62 (2010) 3.
[8] See: W. Sajomsang, Carbohydr. Polym. 80 (2010) 631 and references cited therein.
[9] A. Tolaimate, J. Desbrieres, M. Rhazi, A. Alagui, M. Vincendon, P. Vottero, Polymer 41 (2000) 2463.
[10] M.R. Kasaai, J. Arul, S.L. Chin, G. Charlet, J. Photochem. Photobiol. A: Chem. 120 (1999) 201.
[11] (a) G. Crini, G. Torri, M. Guerrini, M. Morcellet, M. Weltrowski, B. Martel, Carbohydr. Polym. 33 (1997) 145;
(b) R.W.M. Kwok, XPS Peak Fitting Program for WIN95/98 XPSPEAK Version 4.1, Department of Chemistry, The Chinese University of Hong Kong.
[12] C.A. Rodrigues, M.C.M. Laranjeira, V.T. de Favere, E. Stadler, Polymer 39 (1998) 5121.
[13] P.R. Austin, US Patent 4 059 457, 1977.
[14] K. Kurita, Prog. Polym. Sci. 26 (2001) 1921.
[15] K. Kurita, Y. Koyama, K. Murakami, S. Yoshida, N. Chau, Polym. J. 18 (1986) 673.
[16] (a) M.Y. Yin, G.L. Yuan, Y.Q. Wu, M.Y. Huang, Y.Y. Jiang, J. Mol. Catal. A 147 (1999) 93;
(b) A. Corma, P. Concepción, I. Domínguez, V. Fornés, M.J. Sabater, J. Catal. 251 (2007) 39.
[17] (a) G.L. Yuan, M.Y. Yin, T.T. Jiang, M.Y. Huang, Y.Y. Jiang, J. Mol. Catal. A 159 (2000) 45;
(b) K. Tanaka, F. Toda, Chem. Rev. 100 (2000) 1025.
[18] J. Brugnerotto, J. Lizardi, F.M. Goycoolea, W. Arguelles-Monal, J. Desbrieres, M. Rinaudo, Polymer 42 (2001) 3569.
[19] S.E.S. Leonhardt, A. Stolle, B. Ondruschka, G. Cravotto, C. De Leo, K.D. Jandt, T.F. Keller, Appl. Catal. A 379 (2010) 30.
[20] C.C. Romão, F.E. Kühn, W.A. Herrmann, Chem. Rev. 97 (1997) 3197.
[21] J. Mink, G. Keresztury, A. Stirling, W.A. Herrmann, Spectrochim. Acta 50A (1994) 2039.
[22] S.F. Parker, H. Herman, Spectrochim. Acta 56A (2000) 1123.
[23] L. Dambies, C. Guimon, S. Yiacoumi, E. Guibal, Colloids and surfaces A: physicochem, Eng. Aspects 177 (2001) 203.
[24] Y. Yuan, Y. Iwasawa, J. Phys. Chem. B 106 (2002) 4441.
[25] B.M. Choudary, M. Roy, S. Roy, M.L. Kantam, B. Sreedhar, K. Vijay Kumar, Adv. Synth. Catal. 348 (2006) 1734.
[26] W.D. Wang, J.H. Espenson, J. Am. Chem. Soc. 120 (1998) 11335.
[27] C. Mealli, J.A. López, M.J. Calhorda, C.C. Romão, W.A. Herrmann, Inorg. Chem. 33 (1994) 1139.